Assessments of S-NPP and N20 VIIRS DNB and M bands calibration stability and consistency using a homogeneous ground target

Sherry Li*[a], Xiaoxiong Xiong[b]
[a] Science Systems and Applications Inc., 10210 Greenbelt Road, Lanham, MD, 20706
[b] Sciences and Exploration Directorate, NASA/GSFC, Greenbelt, MD, 20771

ABSTRACT

The S-NPP and N20 VIIRS Day-Night band (DNB) and M bands top-of-atmosphere (TOA) radiance and reflectance are calculated and a kernel-driven Bidirectional Reflectance Distribution Function (BRDF) correction model is used to correct the surface and atmosphere combined BRDF influence. Due to degradation in the DNB modulated Relative Spectral Response (RSR), the S-NPP VIIRS observed TOA DNB reflectance indicates a decrease of 1.89% and the SCIAMACHY spectra derived TOA DNB reflectance has a decrease of 1.63% for the past 8.5 years. The N20 VIIRS TOA DNB reflectance decreased 0.50% in the past 2.5 years. The DNB radiance is also compared with the integral of the M bands radiance from M4, M5, and M7. The fitting trends of DNB to the integral of M bands ratios indicate a 0.48% decrease for S-NPP VIIRS and 0.14% increase for N20 VIIRS. The N20 VIIRS DNB to integral M bands ratios are closer to 1 than the S-NPP VIIRS data. The BRDF corrected reflectance comparisons show that the N20 VIIRS data is slightly lower than those of S-NPP VIIRS. The averages of the linear fit values of the N20 to S-NPP VIIRS from 2018 to 2020 June are -1.97%, -4.99%, -3.36%, and -0.85% for M4, M5, M7, and DNB, respectively. Our results indicate that the S-NPP and N20 VIIRS DNB and M bands calibration have been stable. The cross-sensor differences in DNB and M bands are generally consistent with other independent studies using similar and different approaches.

Keywords: Libya 4, Kernel-driven BRDF correction, Integral M bands

1. INTRODUCTION

1.1 S-NPP and N20 VIIRS Sensor Overview

Both Suomi National Polar-orbiting Partnership (S-NPP) and NOAA-20 (N20) are polar orbiting, sun-synchronous satellites. They were launched on October 28, 2011 and November 18, 2017 [1, 2], respectively. The SNPP provides continuity between NASA's Earth Observing System (EOS) satellites and the NOAA Joint Polar Satellite System (JPSS) satellites to observe the Earth, including its land, oceans, and atmosphere [1]. One of the key instruments onboard both S-NPP and N20 is the Visible Infrared Imaging Radiometer Suite (VIIRS). VIIRS has been widely used to collect data of cloud, ocean, land surface, and many other environmental parameters.

VIIRS is designed based on Moderate Resolution Imaging Spectroradiometer (MODIS) heritage with a wide-swath (3030 km) and cross-track scanning radiometer. VIIRS collects Earth's surface data in 22 visible and infrared spectral bands (400-12500 nm). Among the 22 spectral bands, there are 15 Reflective Solar Bands (RSB) and 7 Thermal Emissive Bands (TEB). Among the RSBs, the DNB on VIIRS is a visible/near-infrared panchromatic band. The DNB comprises three gain stages: the low gain stage (LGS), the medium gain stage (MGS), and the high gain stage (HGS); thus, it can observe the Earth during both daytime and nighttime. Scientists have used the DNB for air quality monitoring at night, fire detection, and many other new applications [3, 4]. The S-NPP VIIRS DNB, M4-M7 sensor characteristics are summarized in Table 1. These M bands are used since their spectral ranges are within the wide DNB spectral range. The VIIRS DNB and each M band have 16 detectors; while each I band has 32 detectors in the along-track direction. The VIIRS M bands and I bands detectors are distributed on three Focal Plane Assemblies (FPAs). The DNB detectors are located on a backside-illuminated Charge-Coupled Device (CCD) chip that has three different gain stages [5].

* xuexia.chen@ssaihq.com; phone 1 301 867-2047

Table 1. Sensor characteristics for the S-NPP VIIRS DNB and M4-M7 bands.

VIIRS Band	Central Wavelength (nm)	Bandwidth (nm)	Primary Earth Data Records	Spatial Resolution at Nadir (m)	Gain Stages	Band type
M4	555	20	Ocean Color Aerosols	750	Dual	Visible
M5	672	20	Ocean Color Aerosols	750	Dual	
M6	746	15	Atmospheric Correction	750	Single	Near IR
M7	865	39	Ocean Color Aerosols	750	Dual	
DNB	700	400	Day/Night Band	750	Low Middle High	Visible/ Near IR

1.2 Previous Study on VIIRS Calibration Stability Monitoring

Long term Earth view observations on homogenous targets are often used for monitoring satellite calibration stability. Long term records should be stable if the instrument and ground targets are stable. When records have sharp change or drifts that means new events might have occurred over the sensor operation period, and calibration might need to be updated. The radiometric calibration stability of the VIIRS visible and near infrared spectral bands were evaluated previously using measurements from S-NPP VIIRS over the Libya-4 and Dome C sites [6, 7]. Time series of Deep Convective Clouds were also monitored for the VIIRS DNB and RSB [8, 9]. S-NPP VIIRS has been collecting Earth observation data for more than 8.5 years and N20 VIIRS has been operating for more than 2.5 years. Both instruments are stable as expected from previous long term monitoring studies.

1.3 Objective of This Study

The degradation of N20 VIIRS RSB is much slower than S-NPP because S-NPP VIIRS has the mirror coating contamination of rotating telescope assembly (RTA) [10]. Some studies found that N20 VIIRS is performing as well or slightly better than S-NPP VIIRS [2]. The main objective in this study is to use a ground target, Libya 4, to track the calibration stability of both S-NPP and N20 VIIRS DNB and RSB M4, M5, M7 bands. We cross-compare the two instruments to better understand their performances during their entire missions. The results shown in this paper are useful for validating the current VIIRS instruments calibration stability and can help guide future calibration algorithm improvements and data reprocessing. These methods can be adopted for validating other instruments onboard satellites, such as MODIS and future JPSS satellites.

2. STUDY SITE, DATA, AND METHODOLOGY

2.1 Study Site

The Libya 4 site [Latitude 28.55° N, Longitude: 23.39° E] is a relatively homogeneous site covered by sands in Africa. This ground target is spatially uniform and temporally invariant with stable reflectance and Bidirectional Reflectance Distribution Function (BRDF). This site is located in arid regions and most of the time it has a clear sky perfect for Earth view observations from satellites. Additionally, this desert site has high reflectance in most visible and near infrared bands; thereby it has a high signal-to-noise ratio (SNR) in the data. Fig. 1 shows the Libya 4 site SCIAMACHY spectra,

provided from European Space Agency, and VIIRS pre-launch RSRs for both the S-NPP and N20 VIIRS DNB, M4, M5, and M7 bands. The RSRs from S-NPP and N20 VIIRS have small differences.

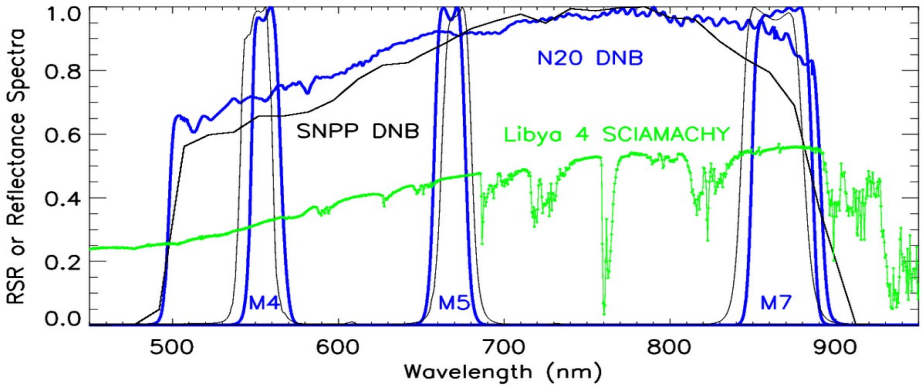

Figure 1. Libya 4 SCIAMACHY spectra (green) and RSRs for the S-NPP (black) and N20 (blue) VIIRS DNB and M bands.

2.2 Data Selection

The data products used in this study are the NASA S-NPP and N20 VIIRS L1B data that can be downloaded from Level 1 and Atmosphere Archive and Distribution System (LAADS) (https://ladsweb.modaps.eosdis.nasa.gov/). We used the S-NPP VIIRS Collection 1 products, Land Science Investigator-led Processing System (LSIPS) Land Archive Set 5000 and also used the N20 VIIRS Collection 2 product, Atmosphere, Land Archive Set 5200. The LSIPS data has been reprocessed with improved calibration algorithms and LUTs (https://landweb.modaps.eosdis.nasa.gov/NPP_QA/). N20 VIIRS Collection 2 data are reprocessed recently.

The data near nadir overpass at the Libya 4 are downloaded for SNPP from 2012 to June 2020, and for N20 from 2018 to June 2020. Any images with clouds, shadows, or heterogeneous surface structures over the Libya 4 site are excluded for this study. Satellite images are investigated both by the covariance filter of the Libya 4 radiance and also by visual check. Data with less homogeneity are excluded if the coefficient of variation (CV) derived from 32x32 pixels is higher than 0.05 for DNB or 0.03 for M bands. The M6 band are excluded in the integral M bands study because the M6 has signal saturation due to a known roll-over issue. The Libya 4 site distances to scene nadir is within 60 DNB pixels (~ 45 km) for S-NPP VIIRS and 118 pixels (~88 km) for N20 VIIRS. The satellite zenith angles are ~1.2-3.4 degrees for S-NPP VIIRS, ~1.9-3.1 degrees for N20 VIIRS nadir left side data, and ~13.3-14.5 degrees for N20 VIIRS nadir right side data. The solar zenith angle range is from 13.5 to 55 degrees for both instruments. Fig. 2 shows the Libya 4 location on SNPP and N20 DNB scenes. Green dash line is the nadir and the center of the scenes.

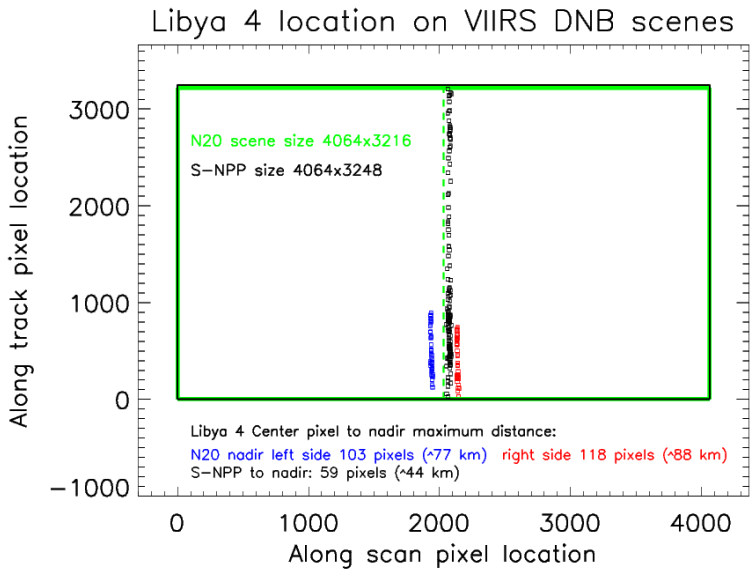

Figure 2. Libya 4 location on SNPP and N20 DNB scenes.

All images are at daytime and the DNB data are all observed in low gain stage at the Libya 4 site. M1-M5 and M7 bands have both high gain and low gain stage observation due to different seasons at the Libya 4 site. Images are selected from 16-day repeatable orbits so all data have similar viewing geometry relative to the site.

Pre-launch RSRs of all VIIRS bands were measured at ambient environment and were provided by the VIIRS Characterization Support Team (VCST). The S-NPP VIIRS modulated RSRs are derived from a wavelength-dependent optical throughput degradation model developed by VCST and were updated based on the needs of RSB LUTs delivery. In this study, N20 VIIRS only has pre-launch RSRs and do not have modulated RSRs.

2.3 Calculate Radiance and Reflectance Data

The DNB and M-bands mean radiances are extracted from 32 by 32 pixels. The extracted DNB pixels are all within the DNB aggregation zone 1. The algorithm used in this study is adapted from previous studies by Chen at al. [7, 11]. The DNB L1B data contains calibrated and geolocated radiance (L_m). The DNB radiance after the Earth-Sun distance and solar zenith angle normalization is calculated for each pixel by using the Eqs. (1) and (2).

$$L_{normalized} = \frac{L_m * d^2}{\cos(\theta)} \quad (1)$$

$L_{\text{normalized}}$ = Measured solar radiance after Earth-Sun distance and solar zenith angle normalization ($W \cdot cm^{-2} \cdot sr^{-1}$)

L_m =Measured solar radiance from the DNB L1B data ($W \cdot cm^{-2} \cdot sr^{-1}$)

d =Earth-Sun distance (astronomical units)

θ =Solar zenith angle (degrees)

$$L_{rsr_{normalized}} = \frac{L_m * d^2}{\cos(\theta) * F_{ESUN}} \quad (2)$$

$$ESUN_t = \frac{\sum (RSR_{\lambda,t} * SolarIrradiance_\lambda * \Delta\lambda)}{\sum (RSR_{\lambda,t} * \Delta\lambda)} \quad (3)$$

$$F_{ESUN} = \frac{ESUN_t}{ESUN_{t0}} \tag{4}$$

$L_{\mathrm{rsr}_{\mathrm{normalized}}}$ = Measured solar radiance after Earth-Sun distance, solar zenith angle, and RSR normalization ($W \cdot cm^{-2} \cdot sr^{-1}$)

F_{ESUN} = Ratio of ESUN between the data collection time t and the reference time t_0 (prelaunch at orbit 154)

ESUN_t=Band dependent and time dependent mean solar irradiance ($W \cdot m^{-2} \cdot nm^{-1}$). The summation is taken over wavelength ranging from 200 nm to 200000 nm.

$\mathrm{SolarIrradiance}_\lambda$ =Solar spectral irradiance ($W \cdot m^{-2} \cdot nm^{-1}$)

$\mathrm{RSR}_{\lambda,t}$ =Wavelength dependent and time dependent RSR of band λ at time t

$\Delta\lambda$ =Wavelength spectral interval (nm)

To retrieve the DNB TOA reflectance data, we use Eq. (5):

$$\rho_{normalized} = \frac{\pi * L_m * d^2}{\cos(\theta) * ESUN_t} \tag{5}$$

$\rho_{\mathrm{normalized}}$=Top of atmosphere reflectance with Earth-Sun distance, solar zenith angle, and RSR normalization.

The M bands L1B data contain both radiance and reflectance data. The M bands radiance ($L_{m_{Mband}}$) ($W \cdot cm^{-2} \cdot sr^{-1}$) and reflectance ($\rho_{normalized_{Mband}}$) data are calculated following Eqs. (6) through (9). The scaled integer (SI), scale, and offset values are provided in the L1B products.

$$L_{m_{Mband}} = SI * scale + offset \tag{6}$$

$$L_{normalized_{Mband}} = \frac{L_{m_{Mband}} * d^2}{\cos(\theta)} \tag{7}$$

$$L_{rsr_{normalized_{Mband}}} = \frac{L_{m_{Mband}} * d^2}{\cos(\theta) * F_{ESUN}} \tag{8}$$

$$\rho_{normalized_{Mband}} = \frac{\pi * L_{m_{Mband}} * d^2}{\cos(\theta) * ESUN_t} \tag{9}$$

2.4 A kernel-driven BRDF correction model

A kernel-driven BRDF model is used in this study. The corrected radiance or reflectance, R, is expressed as Eq. (10) [7, 12]:

$$R^i(\theta_s, \phi_v, \psi) = K_0^i + K_1^i f_1^i(\theta_s, \phi_v, \psi) + K_2^i f_2^i(\theta_s, \phi_v, \psi) \tag{10}$$

where θ, φ are the solar zenith and satellite view zenith angles; ψ is the relative azimuth angle between the solar and satellite sensor directions with values from 0 to π; i is the index for the band wavelength, f_1 is estimated from the bidirectional radiance/reflectance, while f_2 is derived from the volume scattering contribution by a collection of dispersed facets. Coefficients K_0, K_1 and K_2 are parameters related to the surface's subpixel-scale physical structure, optical properties, and the background and protrusion reflectance. The parameter K_0 also represents the bidirectional reflectance at 0 solar zenith angle and view angle, which can provide a basis for the inter-comparison of sensor data acquired with different viewing or solar angles [12]. K_0, K_1 and K_2 are surface type-specific parameters. In this study, we use the 2016 to 2019 four full years available RSR corrected S-NPP VIIRS radiance/reflectance data as the training data set in the kernel-driven BRDF correction model to cover a complete seasonal oscillation cycle. For N20 VIIRS, we use the 2019 July to 2020 June one full year data as training data. In this study, Eq. 11 is used to calculate the BRDF corrected DNB TOA reflectance (ρ_{brdf}) which can be used to validate the long-term sensor calibration stability.

$$\rho_{brdf} = \rho_{normalized} * \frac{K^{i}_{0_{reflec}\tan ce}}{R_{reflec\,\tan ce}} \tag{11}$$

2.5 SCIAMACHY spectral data simulated TOA reflectance

In this study, we also use the Libya 4 spectral data recorded by SCIAMACHY to retrieve the TOA reflectance observed by VIIRS. The SCIAMACHY data used in this study is provided by the European Space Agency. The SCIAMACHY data has a very fine spectral resolution (< 1 nm) and can provide a high spectral precision for our study sites (Fig. 1). We use Eq. (12) [7] to calculate the modulated TOA reflectance considering the RSR influence with time. $\rho_{\text{SCIAMACHY}}$ is the SCIAMACHY spectral reflectance indicated in Fig. 1. The summation is taken over the wavelength parameter λ for each band's RSRs range. We assume that the surface spectral and solar irradiance did not change, and the time dependent RSR is the major source for the change of TOA reflectance.

$$\rho_{TOA_{SCIAMACHY}} = \frac{\sum \left(\rho_{SCIAMACHY} * SolarIrradiance_{\lambda} * RSR_{\lambda} * \Delta\lambda \right)}{\sum \left(RSR_{\lambda} * SolarIrradiance_{\lambda} * \Delta\lambda \right)} \tag{12}$$

First, we use the 8.5 years available S-NPP VIIRS DNB TOA reflectance data (ρ_{brdf}) to generate a linear fit model. Second, we use this linear model to derive fitted reflectance values for all the available dates used in this study. Third, we normalize the ρ_{brdf} and the fitted reflectance data to the first data point of the fitted reflectance. We also normalized the $\rho_{\text{TOA}_{\text{SCIAMACHY}}}$ to its first data point value. After the aforementioned normalization process, the changes of all three data trends can be easily compared. The N20 VIIRS only has pre-launch RSRs, thus its normalized $\rho_{\text{TOA}_{\text{SCIAMACHY}}}$ is always 1 for all bands.

2.6 DNB comparison with integral M bands

In this study, we compare the DNB with the M4, M5, M7 bands. An integrated M bands radiance using M4, M5, and M7 bands are compared with DNB for long term trend monitoring following the equations (13)-(16) [7].

$$R_m = \int RSR(Miband) * RSR(DNB) * \rho \quad * d\lambda$$

$$W_{mi} = \frac{R_{mi}}{R_{m4} + R_{m5} + R_{m7}} \tag{14}$$

$$DNB_{bandwide} = \int RSR(DNB) * d\lambda \tag{15}$$

$$Integral_{Mbands} = (W_{m4} * L_{m4} + W_{m5} * L_{m5} + W_{m7} * L_{m7}) * DNB_{bandwide} \tag{16}$$

R_{mi} (i=4,5,7) are weight parameters of M4, M5, and M7 bands, which are computed from the RSR of these bands [*RSR(Miband)*]. W_{mi} are the adjusted weights that contain the scale factor for making the sum of all the weights equal to 1. The integral M bands radiance ($Integral_{Mbands}$) is calculated in Eq. 16 using the M bands radiance normalized by solar zenith angle, Earth-Sun distance, and BRDF correction (L_{mi}), and the DNB integral RSR ($DNB_{bandwide}$).

3. RESULTS

3.1 Libya 4 site radiance and reflectance long term stability

At the Libya 4 site, the kernel-driven BRDF correction of TOA reflectance can significantly remove the seasonal oscillation, especially for longer wavelengths. The desert site is slightly non-Lambertian, which affects more for the incoming solar irradiance at shorter wavelengths than at longer wavelengths, thus there is reduced scattering and direct reflection at longer wavelengths. In Fig. 3, the DNB reflectance data are normalized to the first fitted value of its linear fit model for both S-NPP and N20 VIIRS. The SCIAMACHY reflectance data are normalized to their first data point. Assuming the surface SCIAMACHY reflectance spectra is stable, the DNB modulated RSR changes will influence the observed TOA reflectance. The SCIAMACHY derived S-NPP VIIRS TOA reflectance shows a 1.63% decrease in the past 8.5 years. The S-NPP VIIRS TOA reflectance trend has some oscillation and the linear fit of the BRDF corrected data indicates a 1.69% decrease in the past. The difference between these two trends is relatively small, which demonstrates that the S-NPP VIIRS DNB reflectance changes are mostly caused by the RSR changes. The SCIAMACHY derived N20 VIIRS DNB TOA reflectance has no changes and the VIIRS data derived TOA reflectance has 0.50% decrease. We need to continue to monitor the long term trends and investigate the N20 VIIRS DNB RSR.

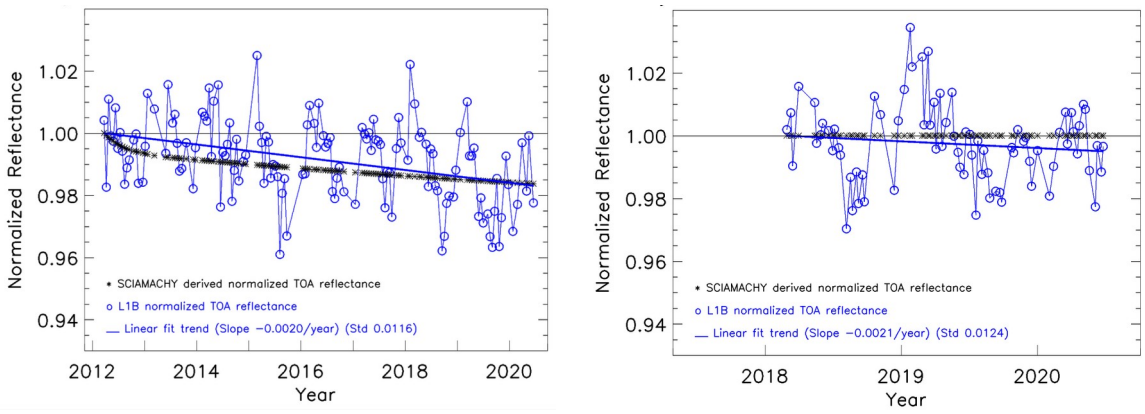

Figure 3. Libya 4 S-NPP (left plot) and N20 (right plot) VIIRS TOA and SCIAMACHY normalized reflectance data.

3.2 DNB and integral M bands comparison

The integral radiance from the M4, M5, and M7 bands are compared with measured DNB radiance after Earth-Sun distance and solar zenith angle correction (Figs. 4 and 5). Their seasonal oscillations are very similar, and the radiance values are close. In the upper plot of Fig. 4, the mean values of S-NPP VIIRS DNB 32x32 pixels' reflectances are indicated in black circles and the integral M bands radiance values are indicated in blue crosses. Their ratios are plotted in the lower part of Fig. 4. The linear fit of the ratio indicated that the slope is about -0.06% per year and the accumulated change of the linear fit values are -0.48% in the past 8.5 years and the DNB is about 1% to 1.48% lower than the integral M bands radiance. Currently, the M bands weights for S-NPP VIIRS are changed with time due to the RSRs change. The N20 VIIRS DNB is about 0.02% higher than the integral M bands radiance. The linear fit of the ratio indicated that the increasing slope is about 0.05% per year and the accumulated change of the linear fit values are 0.14% in the past 2.5 years. These results demonstrate that the instruments are stable as expected.

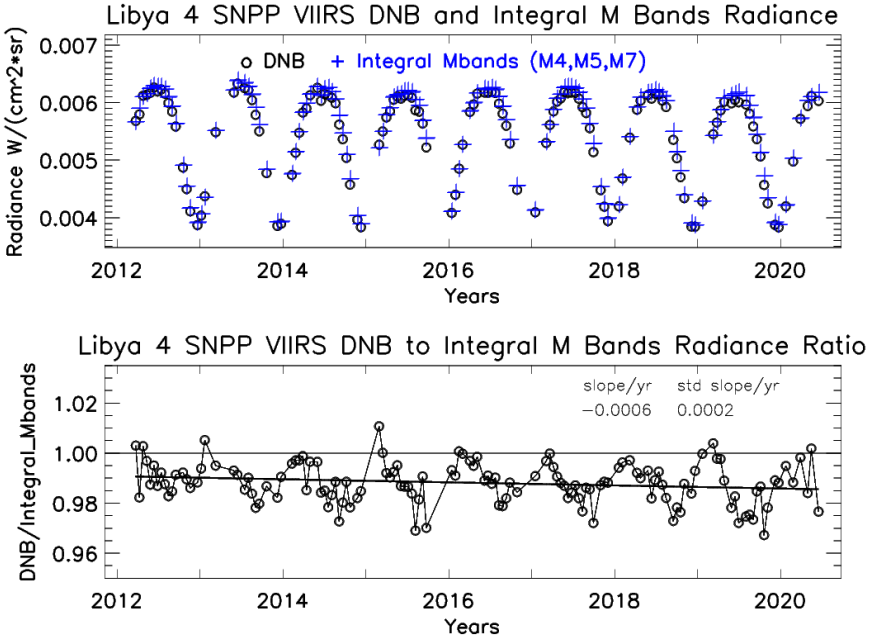

Figure 4. Comparison of Libya 4 S-NPP VIIRS DNB radiance and M bands integral radiance, as well as their ratio.

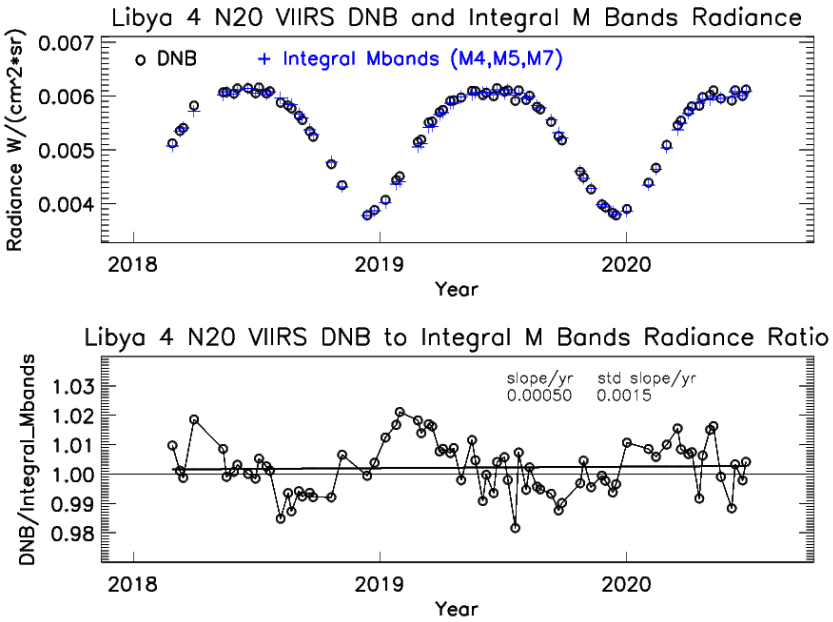

Figure 5. Comparison of Libya 4 N20 VIIRS DNB radiance and M bands integral radiance, as well as their ratio.

3.3 Comparison of S-NPP and N20 reflectance

The S-NPP and N20 VIIRS Libya 4 data are acquired in different solar zenith angle and satellite viewing angles. To cross-compare these two sensors' data, we use the kernel-driven BRDF corrected reflectance data. Fig. 6 indicates the reflectance of DNB and M bands at zero solar zenith angle and view angle after BRDF correction. The ratios of linear fit average value from the N20 to S-NPP for the past 2.5 years are -1.97%, -4.99%, -3.36%, and -0.85% for M4, M5, M7, and DNB, respectively. The DNB observations between the two VIIRS sensors have the less difference among these studied bands. It is caused by the decrease of SNPP DNB reflectance due to modulated RSR changes with time. The cause for these differences is still under investigation. All bands long term trends have a change less than 0.13% per year.

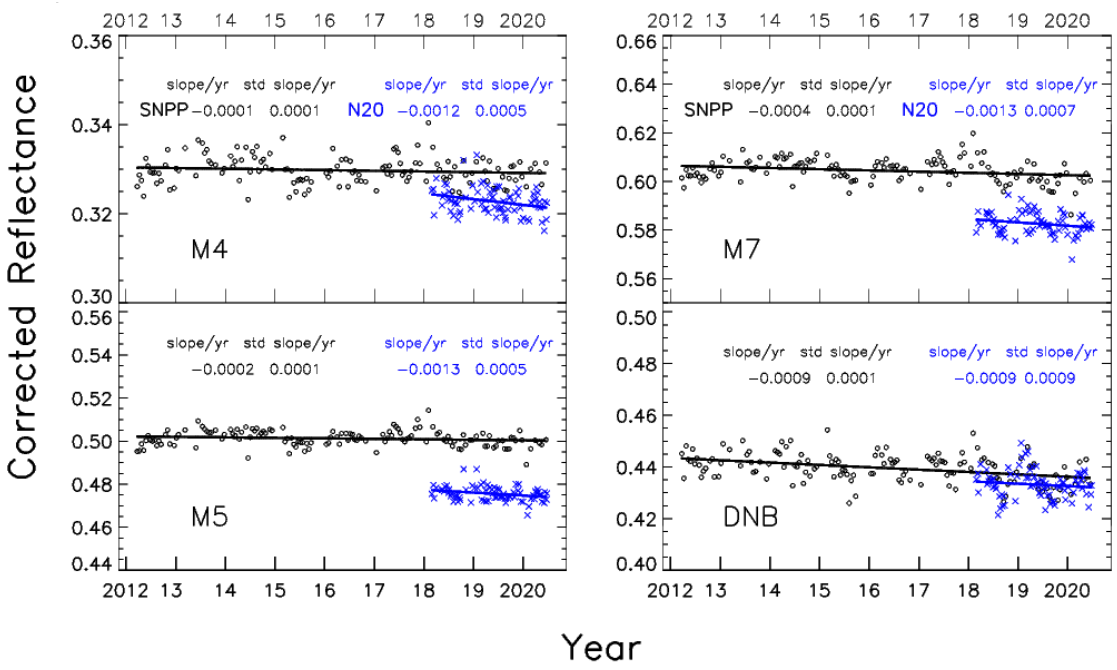

Figure 6. Comparison of Libya 4 S-NPP and N20 VIIRS DNB and M bands BRDF corrected reflectance.

4. CONCLUSIONS

The S-NPP and N20 VIIRS have been collecting observation data for more than 8.5 years and 2.5 years, respectively. Both instruments are stable as expected based on the observation from the long term trends in this study. The Libya 4 site nadir overpass DNB and M bands images are used to validate the instruments calibration performance. The kernel-driven BRDF model is used to remove most of the solar zenith angle and atmospheric Rayleigh scattering influence due to different seasons and atmosphere status in the Libya 4 site.

The S-NPP VIIRS DNB observed TOA reflectance and Libya 4 SCIAMACHY spectra derived TOA reflectance indicate decreasing trends of approximately 1.89% and 1.63% in the past 8.5 years, respectively. Without considering the RSR changes on orbits, the N20 DNB TOA reflectance shows 0.50% decrease in the past 2.5 years. The current DNB trends demonstrate that the S-NPP VIIRS data long-term trend changes are mostly caused by RSR influence.

The DNB and integral M bands comparison indicated that the ratio between these two data are stable for both instruments. The change of the slope is less than 0.06% per year. The N20 DNB to integral M bands ratio are slightly better than S-NPP's ratio. N20 ratio is close to 1.002 while the S-NPP ratio is close to 0.985 in recent linear fit of DNB to integral M bands ratio.

In our investigation, the S-NPP VIIRS DNB modulated RSR introduce an approximately -0.0077 difference at DNB reflectance value in the past 8.5 years. Other M4, M5, M7 bands reflectance has changed -0.0008, -0.0008, and -0.0034, respectively. In the past 2.5 years, the N20 DNB, M4, M5, M7 bands reflectance has changed -0.003, -0.0033, -0.0033, and -0.0023, respectively. SNPP VIIRS reflectance are slightly higher than the N20 reflectance and the largest difference is in M5 (-4.99%) and smallest difference is in DNB (-0.85%).

Though we will need longer VIIRS observation time and more ground data to better understand and verify the S-NPP and N20 VIIRS data quality, results of this study provide useful information on VIIRS post-launch calibration stability and consistency. Based on the above results, both S-NPP and N20 VIIRS data are suitable for long-term monitoring tasks due to its stable radiometric calibration and data reprocessing procedure with improved calibration algorithm. Scientists need to consider the S-NPP VIIRS RSRs degradation influence before using DNB and some other M bands for long-term land cover change detection or monitoring.

ACKNOWLEDGMENTS

The SCIAMACHY spectra data is distributed by the European Space Agency. The authors would like to thank the VCST group internal reviewers for their comments to improve this study.

REFERENCES

[1] Xiong, X., Butler, J., Chiang, K., Efremova, B., Fulbright, J., Lei, N., McIntire, J., Oudrari, H., Wang, Z., and Wu, A., "Assessment of S-NPP VIIRS On-Orbit Radiometric Calibration and Performance," Remote Sensing, 8(2), 84, doi:10.3390/rs8020084 (2016).

[2] Xiong, X., Angal, A., Butler, J., Chen, H., Chiang, K., Lei, N., Li, Y., Twedt, K., "Performance assessments and comparisons of S-NPP and NOAA-20 (JPSS-1) VIIRS On-orbit Calibration," Proc. SPIE 10785, Sensors, Systems, and Next-Generation Satellites XXII, 1078514; doi: 10.1117/12.2326866 (2018).

[3] Wang, J., Aegerter, C., Xu, X., and Szykman, J., "Potential application of VIIRS Day/Night Band for monitoring nighttime surface PM2.5 air quality from space", Atmospheric Environment, Volume 124, Pat A (2016).

[4] Polivka, T., Wang, J., Ellison, L., Hyer, E., and Ichoku, C., "Improving nocturnal fire detection with the VIIRS day–night band," IEEE Trans. Geosci. Remote Sens., vol. 54, no. 9, pp. 5503–5519 (2016).

[5] Northrop Grumman Aerospace Systems, "JPSS VIIRS Radiometric Calibration Algorithm Theoretical Basis Document ATBD," Revision C, https://nsidc.org/sites/nsidc.org/files/technical-references/JPSS-ATBD-VIIRS-SDR-

C.pdf (2014).
[6] Wu, A., Xiong, X., Cao, C., and Chiang, K., “Assessment of SNPP VIIRS VIS/NIR radiometric calibration stability using Aqua MODIS and invariant surface targets”, IEEE Transactions on Geoscience and Remote Sensing, Volume 54, Issue 5, page 2918-2924 (2016).
[7] Chen, X., Wu, A., Xiong, X., Lei, N., Wang, Z., and Chiang, K., “Using ground target to validate S-NPP VIIRS Day-Night Band Calibration”, Remote Sensing, Volume 8, Issue 984 (2016).
[8] Wang, W. and Cao, C., “Monitoring the NOAA operational VIIRS RSB and DNB calibration stability using monthly and semi-monthly deep convective clouds time series”, Remote Sensing, Volume 8, Issue 32, doi:10.3390/rs8010032 (2016).
[9] Chang, T., Xiong, X., and Mu, Q., “VIIRS reflective solar band radiometric and stability evaluation using deep convective clouds,” IEEE Transactions on Geoscience and Remote Sensing, Volume 54, Issue 12, (2016).
[10] Barrie, J.D., Fuqua, P.D., Meshishnek, M.J., Ciofalo, M.R., Chu, C.T., Chaney, J.A., Moision R.M., and Graziani, L., “Root cause determination of on-orbit degradation of the VIIRS rotating telescope assembly,” Earth Observing Systems XIII, Proceedings of SPIE, San Diego, Volume 8510 (2012).
[11] Chen, X., Lei, N., Xiong, X., "Suomi NPP VIIRS DNB and RSB M bands detector-to-detector and HAM side calibration differences assessment using a homogenous ground target," Proc. SPIE 10764, Earth Observing Systems XXIII, 107640X, doi: 10.1117/12.232215 (2018)
[12] Roujean, J.L.; Leroy, M.; and Deschamps, P.Y., “A bidirectional reflectance model of the Earth’s surface for the correction of remote sensing data”. Journal of Geophysical Research. Volume 97, p20455-20468 (1992).